HHS Public Access

Author manuscript

J Am Chem Soc. Author manuscript; available in PMC 2021 March 29.

Published in final edited form as:

J Am Chem Soc. 2019 July 03; 141(26): 10148–10153. doi:10.1021/jacs.9b03329.

Dioxygen-Derived Nonheme Mononuclear Fe^{III}(OH) Complex and Its Reactivity with Carbon Radicals

Vishal Yadav, **Jesse B. Gordon**, **Maxime A. Siegler**, **David P. Goldberg**[*]

Department of Chemistry, The Johns Hopkins University, Baltimore, Maryland 21218, United States

Abstract

A new tetradentate, monoanionic, mixed N/O donor ligand (BNPA^{Ph2}O^{-}) with second coordination sphere H-bonding groups has been synthesized for stabilization of terminal Fe^{III}(OH)(X) complexes. The complex [Fe^{II}(BNPA^{Ph2}O)(OTf)] (**1**) reacts with O_2 to give a mononuclear terminal Fe^{III}(OH) complex, [Fe^{III}(OH)(BNPA^{Ph2}O)(OTf)] (**2**), both of which were characterized by X-ray diffraction, electrospray ionization mass spectrometry, UV–vis, ^{1}H and ^{19}F nuclear magnetic resonance, ^{57}Fe Mössbauer, and electron paramagnetic resonance spectroscopies. Treatment of **2** with carbon radicals ($Ar_3C\cdot$) gives Ar_3COH and the Fe^{II} complex **1**, in direct analogy with the elusive radical "rebound" process proposed for nonheme iron enzymes.

Dioxygen activation at nonheme iron centers is of fundamental importance for a range of enzymatic and synthetic catalysts.[1–3] An archetypal example is seen in the alpha-ketoglutarate (α-KG) dependent nonheme iron enzyme taurine dioxygenase (TauD). The mechanism of TauD involves the binding of O_2 to Fe^{II}, followed by electron transfer from the Fe^{II}/α-KG unit to cleave the O–O bond and give a ferryl (Fe^{IV}(O)) intermediate. The Fe^{IV}(O) species then cleaves the substrate C–H bond to give an Fe^{III}(OH) complex and substrate radical, which recombines via an "oxygen rebound" mechanism to give the final hydroxylated product and the reduced Fe^{II} active site (Scheme 1).[4–8] A related class of nonheme Fe enzymes are the α-KG-dependent halogenases, which exhibit an interesting mechanistic divergence at the ferric hydroxide stage, in which a coordinated halide, or other pseudohalide X (e.g., X = Cl^{-}, Br^{-}, N_3^{-}, NO_2^{-}),[9–13] can preferentially recombine with the substrate radical in lieu of the hydroxide group. Recent efforts to model the latter processes have been described.[14–18] The factors that may bias an Fe^{III}(OH)(X) center toward rebound of X^{-} versus OH^{-} are still not well understood. A similar conundrum arises in the proposed mechanism for isopenicillin N synthase (IPNS), in which a nascent carbon radical recombines with a ligated sulfur center instead of the OH^{-} ligand.[19–21]

[*]**Corresponding Author:** dpg@jhu.edu.

Supporting Information

The Supporting Information is available free of charge on the ACS Publications website at DOI: 10.1021/jacs.9b03329.

X-ray crystallographic data for **1** (CIF)

X-ray crystallographic data for **2** (CIF)

Synthesis, ^{1}H NMR, ^{19}F NMR, ESI-MS, CV, ^{57}Fe Mössbauer data, UV–vis, EPR data, supporting schemes S1–S3, supporting tables S1–S8 and supporting figures S1–S30 (PDF)

The authors declare no competing financial interest.

Our research group has made significant efforts toward constructing inorganic analogs of sulfur-ligated thiol dioxygenases,[22–26] a subclass of nonheme Fe dioxygenases. Part of these efforts has involved discerning the general structural requirements for synthesizing mononuclear Fe^{II} complexes that facilitate O_2 activation. In the course of this work, we have also become interested in examining the factors that contribute to the control of sulfur versus OH rebound in IPNS, as well as more generally, the factors that influence Fe^{III}(OH) reactivity in hydroxylases and halogenases. We recently described the observation of C–O bond formation with a porphyrinoid, formally Fe^{IV}(OH) complex,[27] and a nonheme Fe^{III}(OMe) complex,[28] in reactions with carbon radicals. However, reactivity between an isolated nonheme Fe^{III}(OH) complex and a carbon radical, in direct analogy with the enzymatic processes described in Scheme 1, has not been achieved in any synthetic system to date. Such studies are hampered by the inherent difficulty of synthesizing well-defined, mononuclear Fe^{III}(OH) complexes, which arises in part from their tendency to convert to O(H)-bridged, diferric species.[29,30] Only a relatively small number of mononuclear, nonheme, terminal Fe^{III}(OH) complexes have been structurally characterized.[31–39]

Herein we describe a new tetradentate ligand that was designed to fulfill three criteria: (1) stabilization of an Fe^{III}(OH) unit, (2) O_2 activation at an Fe^{II} center, and (3) inclusion of an open site *cis* to the OH group. This ligand led to the isolation of an Fe^{III}(OH) complex that was obtained via activation of O_2. We can react this complex with exogenous carbon radicals to give the hydroxylated product and the reduced ferrous form, providing a direct analog of the radical “rebound” step in nonheme iron oxygenases.

The new tetradentate ligand $BNPA^{Ph2}OH$, and Fe^{II} complex $Fe^{II}(BNPA^{Ph2}O)(OTf)$ (**1**), were prepared as shown in Scheme 2. The neopentylamine substituents were included as potential stabilizing H-bond donors,[40] a strategy that has been used by others to stabilize metal/oxygen species.[32,33,35,41–44] In addition, an anionic alkoxide donor was installed to facilitate O_2 activation. Metalation with Fe^{II} followed by crystallization gave yellow-green crystals of **1** suitable for X-ray diffraction (XRD). The structure of **1** (Figure 1) reveals a 5-coordinate ($\tau = 0.67$)[45] mononuclear iron(II) complex, with a triflate ligand occupying the fifth site. The neopentyl amine groups are oriented toward the triflate, forming two hydrogen bonds with N1(H)–O2 = 3.026(2) Å and N5(H)–O2 3.116(2) Å.

Complex **1** is pale yellow in CH_3CN, with UV–vis maxima at 323 nm ($\varepsilon = 9550\ M^{-1}\ cm^{-1}$) and 420 nm ($\varepsilon = 990\ M^{-1}\ cm^{-1}$). The ^1H nuclear magnetic resonance (NMR) spectrum of **1** in CD_3CN reveals paramagnetic peaks from +100 to −20 ppm (Figure 2), indicative of a high-spin (hs) Fe^{II} complex. The ^{19}F NMR spectrum in CD_3CN shows a sharp peak at −78 ppm, whereas a broad peak at −74 ppm is observed in tetrahydrofuran (THF)-d_8 (Figure S25), indicative of free and bound triflate ligand, respectively. These data suggest the CD_3CN displaces the OTf^- ligand and the H-bonded site is relatively labile, which would allow for O_2 binding. Mössbauer spectroscopy on solid **1** at 80 K shows a sharp quadrupole doublet with $\delta = 1.03$ and $|\Delta E_Q| = 2.42\ mm\ s^{-1}$, also typical of a hs-$Fe^{II}$ center (Figure S15).

Complex **1** was reacted with excess, dry O_2 gas in CH_3CN at 23 °C, causing an immediate color change from pale yellow to dark orange, with new UV–vis features appearing at 315 nm ($\varepsilon = 9000\ M^{-1}\ cm^{-1}$), 365 nm ($\varepsilon = 2400\ M^{-1}\ cm^{-1}$), and 440 nm ($\varepsilon = 950\ M^{-1}\ cm^{-1}$).

The new dark orange species is air-stable, and the CH_3CN can be removed in vacuo to give an orange solid, which was dissolved in toluene/THF and layered with pentane to afford orange crystals in 24 h that were suitable for XRD.

Analysis by XRD revealed a six-coordinate Fe^{III}(OH) complex, $Fe^{III}(BNPA^{Ph2}O)(OH)(OTf)$ (**2**) (Figure 1). A terminal hydroxide ligand occupies the hydrogen bonding site, and the axial triflate ligand of **1** has shifted to an equatorial position *cis* to the OH^- ligand in **2**. The hydroxide ligand forms two intramolecular hydrogen bonds with the neopentyl amine substituents, with N1(H)–O2 = 2.831(3) and N5(H)–O2 = 2.857(2) Å. There is a third H-bonding interaction between the OH^- and the OTf^- ligands, with O2(H)–O5 = 2.832(1) Å. The Fe–O(H) bond length is 1.880(1)Å, in the range of other H-bonded and non-H-bonded Fe^{III}(OH) complexes.[31–35] However, a proper comparison with a non-H-bonded analog of **2** is currently not available. The $Fe–N_{py}$ and $Fe–N_{amine}$ distances are shorter by 0.1–0.2 Å when compared to the Fe^{II} analog **1**, and the Fe–O1 distance is also contracted by 0.05 Å.

Complex **2** shows paramagnetic peaks in the ^1H NMR spectrum from 150 to 1 ppm (Figure 2). The ^{19}F NMR spectrum for **2** in CD_3CN shows a sharp peak at −74.6 ppm, which corresponds to free OTf^-, and indicates the OTf^- ligand is likely displaced by solvent. In contrast, the same spectrum in the more weakly coordinating THF-d_8 shows no peaks from +200 to −200 ppm, consistent with OTf^- remaining coordinated (Figure S26). The EPR spectrum (20 K) reveals signals at $g = 9.01, 4.23$, which is consistent with an $S = 5/2$ ferric ion (Figure S14). Analysis of a crystalline sample of **2** by Mössbauer spectroscopy at 80 K reveals a broad quadrupole doublet which can be fit with $\delta = 0.47$ mm s^{-1} and $|\Delta E_Q| = 0.97$ mm s^{-1} (Figure S16). The broadened spectrum comes from **2** likely being in an intermediate spin relaxation regime.[46,47] The Mössbauer spectrum of **2** at 5 K shows a 6 line hyperfine splitting pattern which is expected for a high-spin Fe^{III} species (Figure S17).

Density functional theory (DFT) was employed to obtain optimized structures for **1** and **2** at the BP86/6–311G*/6–31G* (for C and H atoms) level of theory. These optimized structures matched well with the structures from XRD for **1** and **2**, and were then used for the calculation of Mössbauer spectroscopic parameters. The calculations gave $\delta = 1.05$ and $|\Delta E_Q| = 2.61$ mm s^{-1} for **1**, and $\delta = 0.47$ and $|\Delta E_Q| = 1.42$ mm s^{-1} for **2**. These parameters are in reasonable agreement with experiment for the solid-state samples.

Production of **2** by addition of excess O_2 in acetonitrile followed by electrospray ionization mass spectrometry (ESI-MS) reveals the major peak at $m/z = 636.85$ (positive ion mode), corresponding to $[\mathbf{2}–OTf]^+$. In comparison, the use of isotopically labeled $^{18}O_2$ leads to the major peak shifted by +2 units to $m/z = 638.85$. Addition of excess $H_2{}^{18}O$ to **1** in CH_3CN, followed by exposure to excess, natural abundance O_2, does not lead to any shift in the major peak at m/z 636.85. These ^{18}O-labeling experiments show that the hydroxide ligand must originate from dioxygen.

A suggested mechanism is given in Scheme S1. Initial binding of O_2 gives an Fe^{III}(superoxo) species that then leads to a peroxo-bridged dimer, followed by homolytic O–O cleavage to give an Fe^{IV}(O) species. The latter species then abstracts hydrogen from an exogenous source (e.g., solvent) to give **2**. Precedent for this mechanism is described for

both heme and nonheme Fe and Mn complexes.[33,48–50] Carrying out the reaction of **1** with O_2 in the presence of excess 9,10-dihydroanthracene, a potential H atom donor, leads to production of anthracene in ~90% yield (Scheme 3), consistent with H atom abstraction by the putative ferryl intermediate. Attempts to observe intermediates in the reaction between **1** and O_2 were carried out at lower temperature. However, at temperatures as low as −90 °C, only the formation of **2** was observed as seen at 23 °C, and at lower temperatures (e.g., −105 °C) no reaction occurs.

The similarity of complex **2** to the enzymatic species shown in Scheme 1 motivated us to examine its reactivity with carbon-based radicals. Addition of $Ph_3C\cdot$ to **2** in THF at 23 °C causes a color change from dark orange to yellow over 4 h. The ^{1}H NMR spectrum shows complete loss of **2**, and the appearance of peaks for **1** (Figure 2). A new peak at δ 5.50 ppm was also formed, arising from the alcohol (Ph_3COH) in 84% (±3) yield (Scheme 4).

Changing to the more electron-rich (p-OMe-C_6H_4)3C· (1 equiv) causes faster conversion (~45 min) of **2** to **1** as seen by ^{1}H NMR spectroscopy. Quantification of (p-OMe-$C_6H_4)_3COH$ gives a yield of 87% (±2) (Scheme 4), consistent with 1:1 stoichiometry between **2** and the radical.

The formation of the products (p-X-C6$H_4)_3COH$ (X = H, OMe) was also confirmed by ESI-MS analysis (Figures S22 and 23). Incorporation of ^{18}OH into **2** by exchange with $H_2{}^{18}O$ was quantitative, and reaction of (p-X-$C_6H_4)_3C\cdot$ (X = H, OMe) with ^{18}O-labeled **2**, led to a two unit shift in m/z by ESI-MS analysis (Figures S28 and 29, ^{18}O incorporation, 99%)). These results indicate that there is direct transfer of the OH ligand to the carbon radicals.

The reaction with the p-OMe derivative was monitored by Mössbauer spectroscopy (Figure 3). The spectrum for ^{57}Fe-labeled complex **1** in 2-MeTHF(80 K) gives δ = 1.14 mm s^{-1} and $|\Delta E_Q|$ = 2.24 mm s^{-1} (Figure 3a). The spectrum for complex **2** (Figure 3b) is broad, with δ = 0.47 mm s^{-1} and $|\Delta E_Q|$ = 1.24 mm s^{-1} (see Figure S18 for fitting details). Reaction between **2** and (p-OMe-$C_6H_4)_3C\cdot$ gives a quadrupole doublet matching **1** (δ = 1.14 mm s^{-1}; $|\Delta E_Q|$ = 2.23 mm s^{-1}) (Figure 3c), which accounts for 90% of the total Fe.

Electrochemical analysis of **2** shows a reversible wave in the cyclic voltammogram with $E_{1/2}$ = −0.69 V (ΔE_{pp} = 170 mV) vs Fc^+/Fc in CH_3CN. This reduction potential is in line with other Fe^{III}(OH) complexes (Table S8). The redox potentials for (p-X-$C_6H_4)_3C^+$/(p-X-$C_6H_4)_3C\cdot$ are −0.11 V (X = H) and −0.58 V (X = OMe), in the same solvent,[51] indicating that outer-sphere electron-transfer (ET) from (p-X-$C_6H_4)_3C\cdot$ to **2** should be endergonic by 13.4 kcal mol^{-1} for X = H, and 2.5 kcal mol^{-1} for X = OMe. Thus, ET to **2** is thermodynamically unfavorable for both carbon radicals, suggesting that a concerted process may be operative (Scheme S2).

In conclusion, the incorporation of an anionic donor combined with H-bond groups in the second coordination sphere of a new tetradentate ligand provided access to an Fe^{II} complex that activates O_2 and yields a stable, terminal Fe^{III}(OH) complex. Reaction of the latter complex with trityl radical derivatives led to the first direct observation[52] of a model “rebound” reaction to give the hydroxylated carbon product and the one-electron-reduced

Fe^{II} complex. It may be somewhat surprising that smooth transfer of $OH^{\bullet}$ from Fe to the radical occurs, because of the significant steric encumbrance and tight H-bond network in **2**. Determining what inherent factors (e.g., H-bonding, sterics, redox potential, donor atoms) influence O_2 activation and Fe(OH)/radical reactivity will be the focus of future studies.

In addition, the new $BNPA^{Ph2}O^{-}$ ligand leaves a potential labile equatorial site on the metal to build Fe(OH)(X) complexes. Efforts to replace the equatorial OTf^{-} in 2 with other anionic donors are underway.

Supplementary Material

Refer to Web version on PubMed Central for supplementary material.

ACKNOWLEDGMENTS

The NIH (GM119374 to D.P.G.) is gratefully acknowledged for financial support. Computer time was provided by the Maryland Advanced Research Computing Center (MARCC). We also thank Prof. Guy N. L. Jameson for valuable discussions.

REFERENCES

(1). Sahu S; Goldberg DP Activation of Dioxygen by Iron and Manganese Complexes: A Heme and Nonheme Perspective. J. Am. Chem. Soc 2016, 138, 11410–28. [PubMed: 27576170]

(2). Kovaleva EG; Lipscomb JD Versatility of biological nonheme Fe(II) centers in oxygen activation reactions. Nat. Chem. Biol 2008, 4, 186–93. [PubMed: 18277980]

(3). Hong S; Lee Y-M; Ray K; Nam W Dioxygen activation chemistry by synthetic mononuclear nonheme iron, copper and chromium complexes. Coord. Chem. Rev 2017, 334, 25–42.

(4). Mitchell AJ; Dunham NP; Martinie RJ; Bergman JA; Pollock CJ; Hu K; Allen BD; Chang W.-c.; Silakov A; Bollinger JM Jr.; Krebs C; Boal AK Visualizing the Reaction Cycle in an Iron(II)- and 2-(Oxo)-glutarate-Dependent Hydroxylase. J. Am. Chem. Soc 2017, 139, 13830–13836. [PubMed: 28823155]

(5). Bollinger JM Jr.; Chang W.-c.; Matthews ML; Martinie RJ; Boal AK; Krebs C Chapter 3. Mechanisms of 2-Oxoglutarate-Dependent Oxygenases: The Hydroxylation Paradigm and Beyond. In 2-Oxoglutarate-Dependent Oxygenases; Schofield CJ, Hausinger RP, Eds.; The Royal Society of Chemistry, 2015; pp 95–122.

(6). Martinez S; Hausinger RP Catalytic Mechanisms of Fe(II)- and 2-Oxoglutarate-Dependent Oxygenases. J. Biol. Chem 2015, 290, 20702–11. [PubMed: 26152721]

(7). Timmins A; de Visser SP A Comparative Review on the Catalytic Mechanism of Nonheme Iron Hydroxylases and Halogenases. Catalysts 2018, 8, 314.

(8). Wojcik A; Radon M; Borowski T Mechanism of O_2 Activation by alpha-Ketoglutarate Dependent Oxygenases Revisited. A Quantum Chemical Study. J. Phys. Chem. A 2016, 120, 1261–74. [PubMed: 26859709]

(9). Matthews ML; Neumann CS; Miles LA; Grove TL; Booker SJ; Krebs C; Walsh CT; Bollinger JM Jr. Substrate positioning controls the partition between halogenation and hydroxylation in the aliphatic halogenase, SyrB2. Proc. Natl. Acad. Sci. U. S. A 2009, 106, 17723–8. [PubMed: 19815524]

(10). Matthews ML; Chang WC; Layne AP; Miles LA; Krebs C; Bollinger JM Jr. Direct nitration and azidation of aliphatic carbons by an iron-dependent halogenase. Nat. Chem. Biol 2014, 10, 209–15. [PubMed: 24463698]

(11). Timmins A; Quesne MG; Borowski T; de Visser SP Group Transfer to an Aliphatic Bond: A Biomimetic Study Inspired by Nonheme Iron Halogenases. ACS Catal. 2018, 8, 8685–8698.

(12). Pratter SM; Ivkovic J; Birner-Gruenberger R; Breinbauer R; Zangger K; Straganz GD More than just a Halogenase: Modification of Fatty Acyl Moieties by a Trifunctional Metal Enzyme. ChemBioChem 2014, 15, 567–574 [PubMed: 24497159]

(13). Mitchell AJ; Dunham NP; Bergman JA; Wang B; Zhu Q; Chang W-c.; Liu, X.; Boal, A. K. Structure-Guided Reprogramming of a Hydroxylase To Halogenate Its Small Molecule Substrate. Biochemistry 2017, 56, 441–444. [PubMed: 28029241]

(14). Puri M; Biswas AN; Fan R; Guo Y; Que L Jr. Modeling Non-Heme Iron Halogenases: High-Spin Oxoiron(IV)–Halide Complexes That Halogenate C–H Bonds. J. Am. Chem. Soc 2016, 138, 2484–2487. [PubMed: 26875530]

(15). Planas O; Clémancey M; Latour J-M; Company A; Costas M Structural modeling of iron halogenases: synthesis and reactivity of halide-iron(iv)-oxo compounds. Chem. Commun 2014, 50, 10887–10890.

(16). Rana S; Biswas JP; Sen A; Clémancey M; Blondin G; Latour J-M; Rajaraman G; Maiti D Selective C–H halogenation over hydroxylation by non-heme iron(iv)-oxo. Chem. Sci 2018, 9, 7843–7858. [PubMed: 30429994]

(17). Rana S; Bag S; Patra T; Maiti D Catalytic Electrophilic Halogenations and Haloalkoxylations by Non-Heme Iron Halides. Adv. Synth. Catal 2014, 356, 2453–2458.

(18). Chatterjee S; Paine TK Hydroxylation versus Halogenation of Aliphatic C–H Bonds by a Dioxygen-Derived Iron–Oxygen Oxidant: Functional Mimicking of Iron Halogenases. Angew. Chem., Int. Ed 2016, 55, 7717–7722.

(19). Tamanaha E; Zhang B; Guo Y; Chang WC; Barr EW; Xing G; St. Clair J; Ye S; Neese F; Bollinger JM Jr.; Krebs C Spectroscopic Evidence for the Two C-H-Cleaving Intermediates of Aspergillus nidulans Isopenicillin N Synthase. J. Am. Chem. Soc 2016, 138, 8862–8874. [PubMed: 27193226]

(20). Ge W; Clifton IJ; Stok JE; Adlington RM; Baldwin JE; Rutledge PJ Isopenicillin N Synthase Mediates Thiolate Oxidation to Sulfenate in a Depsipeptide Substrate Analogue: Implications for Oxygen Binding and a Link to Nitrile Hydratase? J. Am. Chem. Soc 2008, 130, 10096–10102. [PubMed: 18620394]

(21). Kawatsu T; Lundberg M; Morokuma K Protein Free Energy Corrections in ONIOM QM:MM Modeling: A Case Study for Isopenicillin N Synthase (IPNS). J. Chem. Theory Comput 2011, 7, 390–401. [PubMed: 26596161]

(22). Gordon JB; Vilbert AC; Siegler MA; Lancaster KM; Moënne-Loccoz P; Goldberg DP A Nonheme Thiolate-Ligated Cobalt Superoxo Complex: Synthesis and Spectroscopic Characterization, Computational Studies, and Hydrogen Atom Abstraction Reactivity. J. Am. Chem. Soc 2019, 141, 3641–53. [PubMed: 30776222]

(23). Badiei YM; Siegler MA; Goldberg DP O_2 activation by bis(imino)pyridine iron(II)-thiolate complexes. J. Am. Chem. Soc 2011, 133, 1274–7. [PubMed: 21207980]

(24). Gordon JB; McGale JP; Prendergast JR; Shirani-Sarmazeh Z; Siegler MA; Jameson GNL; Goldberg DP Structures, Spectroscopic Properties, and Dioxygen Reactivity of 5- and 6-Coordinate Nonheme Iron(II) Complexes: A Combined Enzyme/Model Study of Thiol Dioxygenases. J. Am. Chem. Soc 2018, 140, 14807–14822. [PubMed: 30346746]

(25). McQuilken AC; Jiang Y; Siegler MA; Goldberg DP Addition of Dioxygen to an N4S(thiolate) Iron(II) Cysteine Dioxygenase Model Gives a Structurally Characterized Sulfinato–Iron(II) Complex. J. Am. Chem. Soc 2012, 134, 8758–8761. [PubMed: 22578255]

(26). Jiang Y; Widger LR; Kasper GD; Siegler MA; Goldberg DP Iron(II)-Thiolate S-Oxygenation by O_2: Synthetic Models of Cysteine Dioxygenase. J. Am. Chem. Soc 2010, 132, 12214–12215. [PubMed: 20712312]

(27). Zaragoza JPT; Yosca TH; Siegler MA; Moënne-Loccoz P; Green MT; Goldberg DP Direct Observation of Oxygen Rebound with an Iron-Hydroxide Complex. J. Am. Chem. Soc 2017, 139, 13640–13643. [PubMed: 28930448]

(28). Pangia TM; Davies CG; Prendergast JR; Gordon JB; Siegler MA; Jameson GNL; Goldberg DP Observation of Radical Rebound in a Mononuclear Nonheme Iron Model Complex. J. Am. Chem. Soc 2018, 140, 4191–4194. [PubMed: 29537258]

(29). Brines LM; Coggins MK; Poon PCY; Toledo S; Kaminsky W; Kirk ML; Kovacs JA Water-Soluble Fe(II)–H_2O Complex with a Weak O–H Bond Transfers a Hydrogen Atom via an Observable Monomeric Fe(III)–OH. J. Am. Chem. Soc 2015, 137, 2253–2264. [PubMed: 25611075]

(30). Ching W-M; Zhou A; Klein JEMN; Fan R; Knizia G; Cramer CJ; Guo Y; Que L Jr. Characterization of the Fleeting Hydroxoiron(III) Complex of the Pentadentate TMC-py Ligand. Inorg. Chem 2017, 56, 11129–11140. [PubMed: 28858496]

(31). Ogo S; Wada S; Watanabe Y; Iwase M; Wada A; Harata M; Jitsukawa K; Masuda H; Einaga H Synthesis, Structure, and Spectroscopic Properties of [FeIII(tnpa)(OH)(PhCOO)]ClO_4: A Model Complex for an Active Form of Soybean Lipoxygenase-1. Angew. Chem., Int. Ed 1998, 37, 2102–2104.

(32). Ogo S; Yamahara R; Roach M; Suenobu T; Aki M; Ogura T; Kitagawa T; Masuda H; Fukuzumi S; Watanabe Y Structural and Spectroscopic Features of a cis (Hydroxo)-FeIII-(Carboxylato) Configuration as an Active Site Model for Lipoxygenases. Inorg. Chem 2002, 41, 5513–5520. [PubMed: 12377047]

(33). MacBeth CE; Golombek AP; Young VG; Yang C; Kuczera K; Hendrich MP; Borovik AS Activation by Nonheme Iron Complexes: A Monomeric Fe(III)-Oxo Complex Derived From O_2. Science 2000, 289, 938. [PubMed: 10937994]

(34). Çelenligil-Çetin R; Paraskevopoulou P; Dinda R; Staples RJ; Sinn E; Rath NP; Stavropoulos P Synthesis, Characterization, and Reactivity of Iron Trisamidoamine Complexes That Undergo Both Metal- and Ligand-Centered Oxidative Transformations. Inorg. Chem 2008, 47, 1165–1172. [PubMed: 18179206]

(35). Soo HS; Komor AC; Iavarone AT; Chang CJ A Hydrogen-Bond Facilitated Cycle for Oxygen Reduction by an Acid- and Base-Compatible Iron Platform. Inorg. Chem 2009, 48, 10024–10035. [PubMed: 19780564]

(36). Cook SA; Ziller JW; Borovik AS Iron(II) Complexes Supported by Sulfonamido Tripodal Ligands: Endogenous versus Exogenous Substrate Oxidation. Inorg. Chem 2014, 53, 11029–11035. [PubMed: 25264932]

(37). Kleinlein C; Bendelsmith AJ; Zheng S-L; Betley TA C–H Activation from Iron(II)-Nitroxido Complexes. Angew. Chem., Int. Ed 2017, 56, 12197–12201.

(38). Chambers MB; Groysman S; Villagrán D; Nocera DG Iron in a Trigonal Tris(alkoxide) Ligand Environment. Inorg. Chem 2013, 52, 3159–3169. [PubMed: 23432161]

(39). Mukherjee J; Lucas RL; Zart MK; Powell DR; Day VW; Borovik AS Synthesis, Structure, and Physical Properties for a Series of Monomeric Iron(III) Hydroxo Complexes with Varying Hydrogen-Bond Networks. Inorg. Chem 2008, 47, 5780–5786. [PubMed: 18498155]

(40). Berreau LM; Allred RA; Makowska-Grzyska MM; Arif AM Synthesis and structure of a nitrogen/sulfur-ligated zinc hydroxide complex. Chem. Commun 2000, 1423–1424.

(41). Ford CL; Park YJ; Matson EM; Gordon Z; Fout AR A bioinspired iron catalyst for nitrate and perchlorate reduction. Science 2016, 354, 741–43. [PubMed: 27846604]

(42). Gordon Z; Drummond MJ; Matson EM; Bogart JA; Schelter EJ; Lord RL; Fout AR Tuning the Fe(II/III) Redox Potential in Nonheme Fe(II)–Hydroxo Complexes through Primary and Secondary Coordination Sphere Modifications. Inorg. Chem 2017, 56, 4852–4863. [PubMed: 28394119]

(43). Dahl EW; Dong HT; Szymczak NK Phenylamino derivatives of tris(2-pyridylmethyl)amine: hydrogen-bonded perox-odicopper complexes. Chem. Commun 2018, 54, 892–895.

(44). Dahl EW; Kiernicki JJ; Zeller M; Szymczak NK Hydrogen Bonds Dictate O_2 Capture and Release within a Zinc Tripod. J. Am. Chem. Soc 2018, 140, 10075–10079. [PubMed: 30074788]

(45). Addison AW; Rao TN; Reedijk J; van Rijn J; Verschoor GC Synthesis, structure, and spectroscopic properties of copper(II) compounds containing nitrogen–sulphur donor ligands; the crystal and molecular structure of aqua[1,7-bis(N-methylbenzimidazol-2′-yl)-2,6-dithiaheptane]copper(II) perchlorate. J. Chem. Soc., Dalton Trans 1984, 1349–1356.

(46). Mørup S Magnetic Relaxation Phenomena. In Mössbauer Spectroscopy and Transition Metal Chemistry: Fundamentals and Applications; Gütlich P, Bill E, Trautwein AX, Eds.; Springer: Berlin, Heidelberg, 2011; pp 201–234.

(47). Gupta R; Lacy DC; Bominaar EL; Borovik AS; Hendrich MP Electron Paramagnetic Resonance and Mössbauer Spectroscopy and Density Functional Theory Analysis of a High-Spin FeIV–Oxo Complex. J. Am. Chem. Soc 2012, 134, 9775–9784. [PubMed: 22574962]

(48). Wijeratne GB; Corzine B; Day VW; Jackson TA Saturation Kinetics in Phenolic O–H Bond Oxidation by a Mononuclear Mn(III)–OH Complex Derived from Dioxygen. Inorg. Chem 2014, 53, 7622–7634. [PubMed: 25010596]

(49). Lee Y-M; Hong S; Morimoto Y; Shin W; Fukuzumi S; Nam W Dioxygen Activation by a Non-Heme Iron(II) Complex: Formation of an Iron(IV)–Oxo Complex via C–H Activation by a Putative Iron(III)–Superoxo Species. J. Am. Chem. Soc 2010, 132, 10668–10670. [PubMed: 20681694]

(50). Kim SO; Sastri CV; Seo MS; Kim J; Nam W Dioxygen Activation and Catalytic Aerobic Oxidation by a Mononuclear Nonheme Iron(II) Complex. J. Am. Chem. Soc 2005, 127, 4178–4179. [PubMed: 15783193]

(51). Volz H; Lotsch W Polarographische reduktion von triarylmethylkationen. Tetrahedron Lett. 1969, 10, 2275–2278.

(52). While this paper was under review, a report of a nonheme Fe^{III}(OH) complex reacting with (p-H-$C_6H_4)_3C\cdot$ to give Fe^{II} and alcohol was described Drummond MJ; Ford CL; Gray DL; Popescu CV; Fout AR J. Am. Chem. Soc 2019, 141, 6639–6650. [PubMed: 30969766]

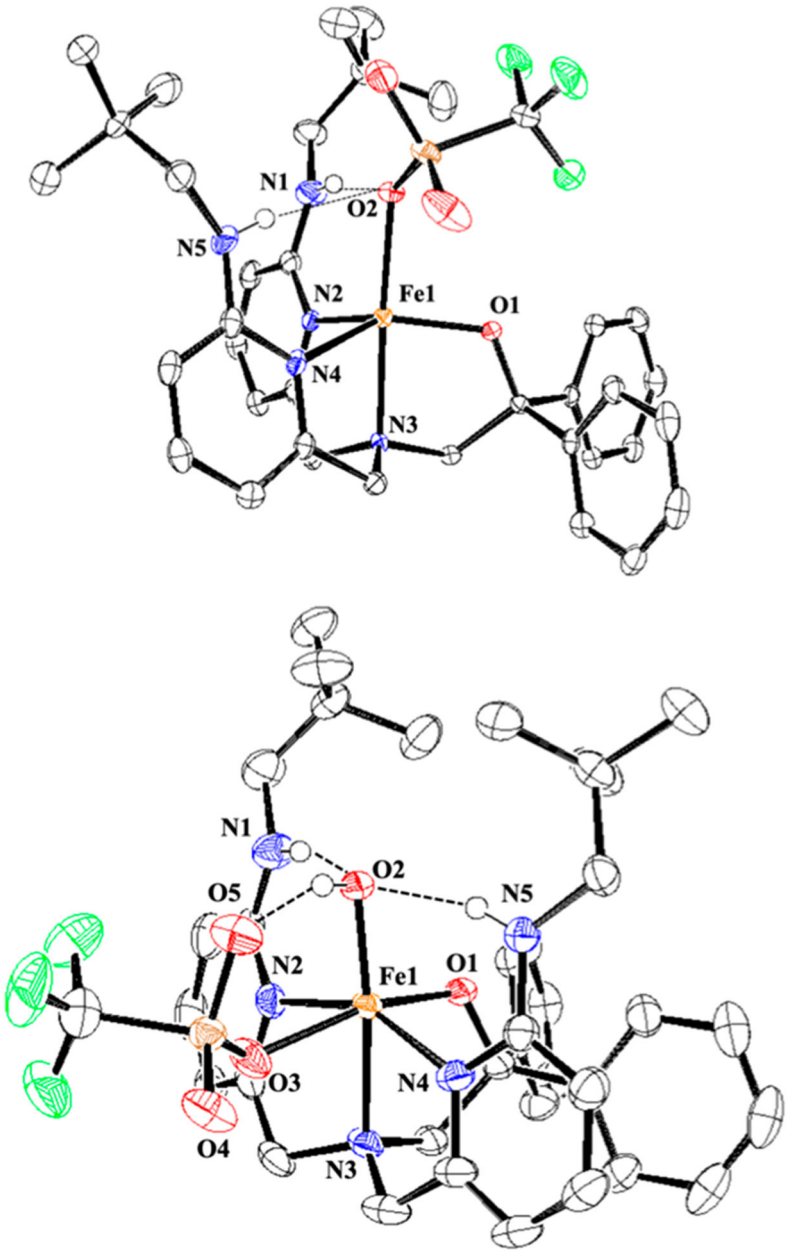

Figure 1.

Displacement ellipsoid plots (50% probability level) for **1** and **2** at 110(2) K. Hydrogen atoms (except for N–H and O–H) have been omitted for clarity.

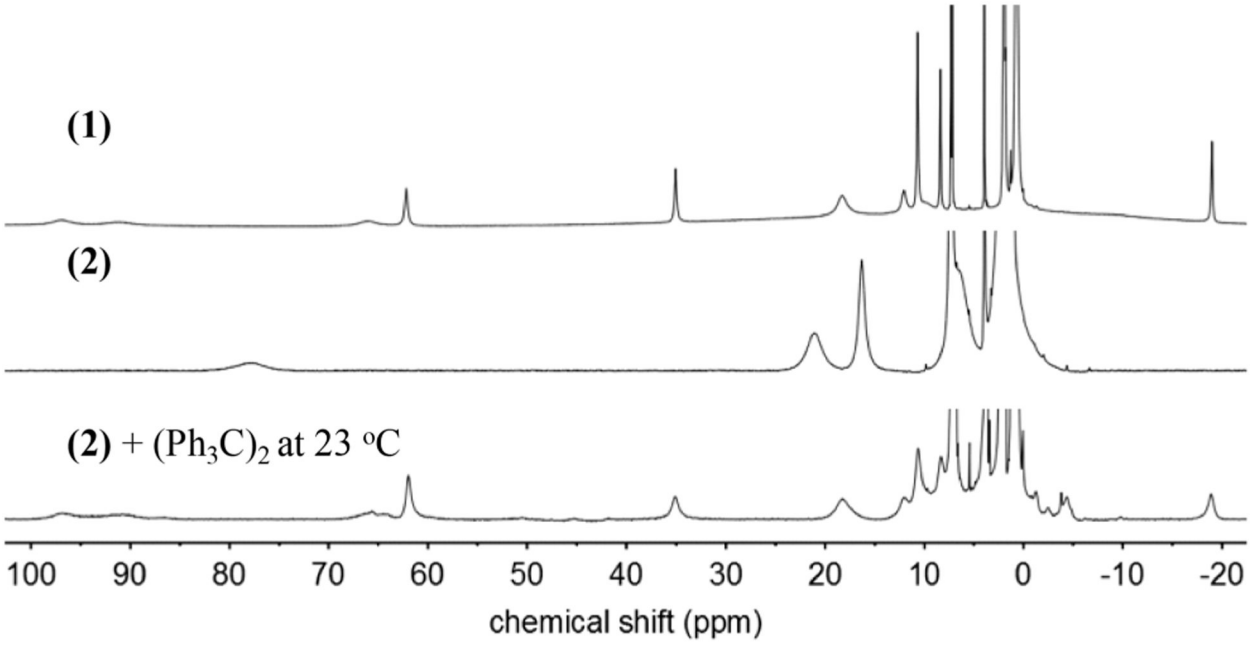

Figure 2.

^{1}H NMR spectra (CD_3CN) of **1** (top), **2** (middle), and reaction of **2** with excess $(Ph_3C)_2$ (bottom) after removal of THF and dissolution in CD_3CN.

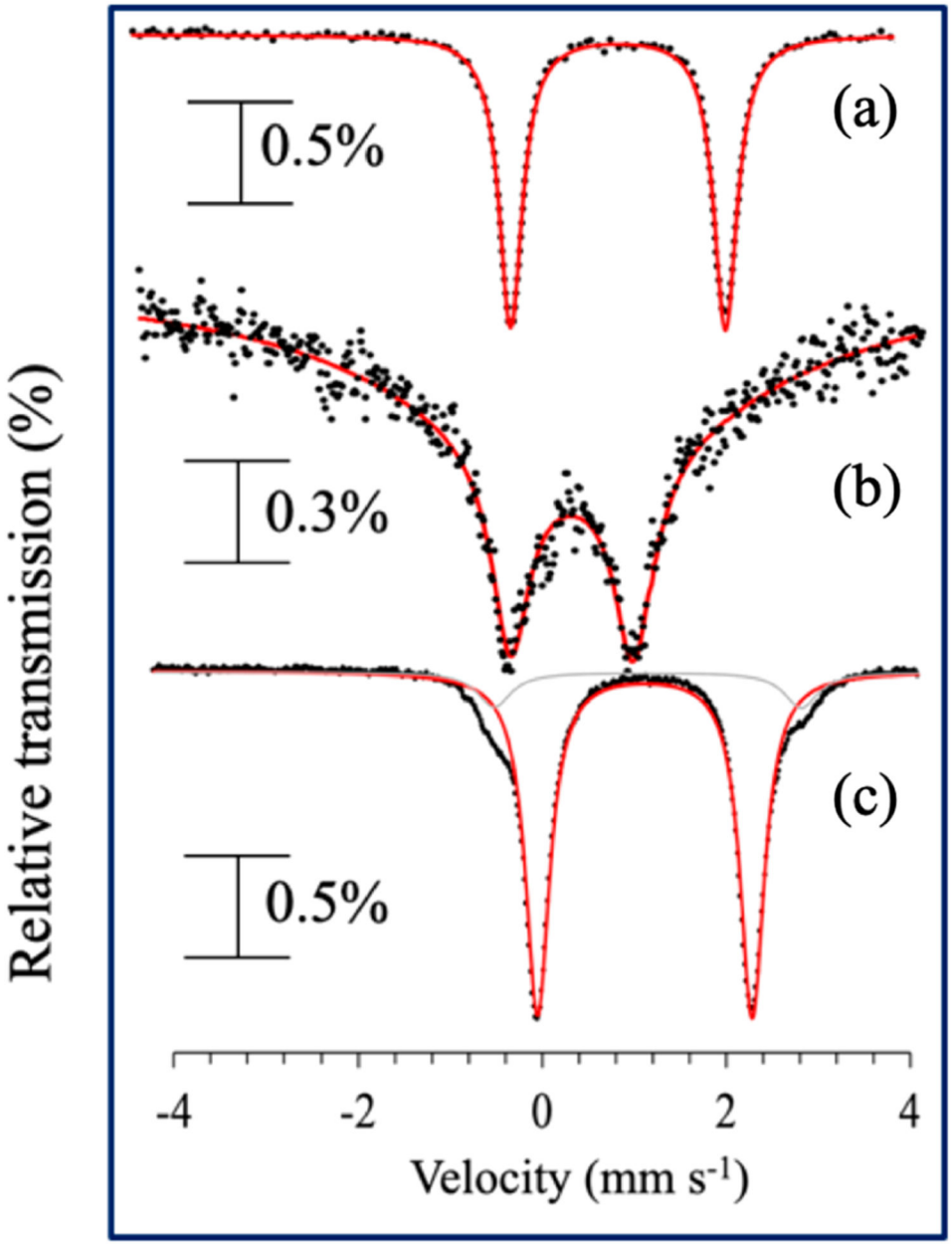

Figure 3.
Zero field ^{57}Fe Mössbauer spectra (80 K) of (a) **1**, (b) **2** in 2-MeTHF, and (c) reaction of **2** with (p-OMe-$C_6H_4)_3C\cdot$ (at 23 °C) in 2-MeTHF. Black circles = experimental data; red line = best fit.

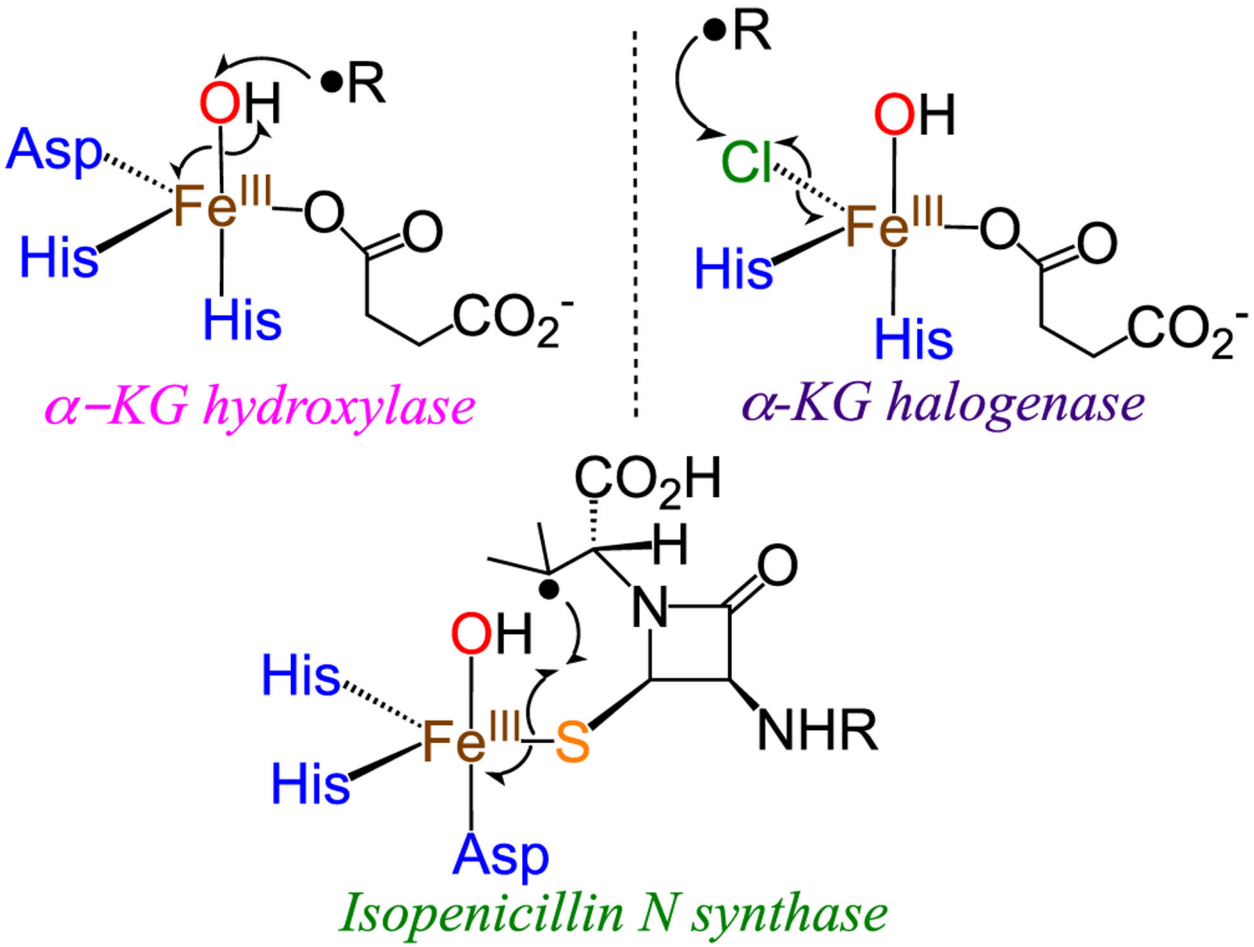

Scheme 1.
Selective Rebound Step in Different Nonheme Iron Enzymes

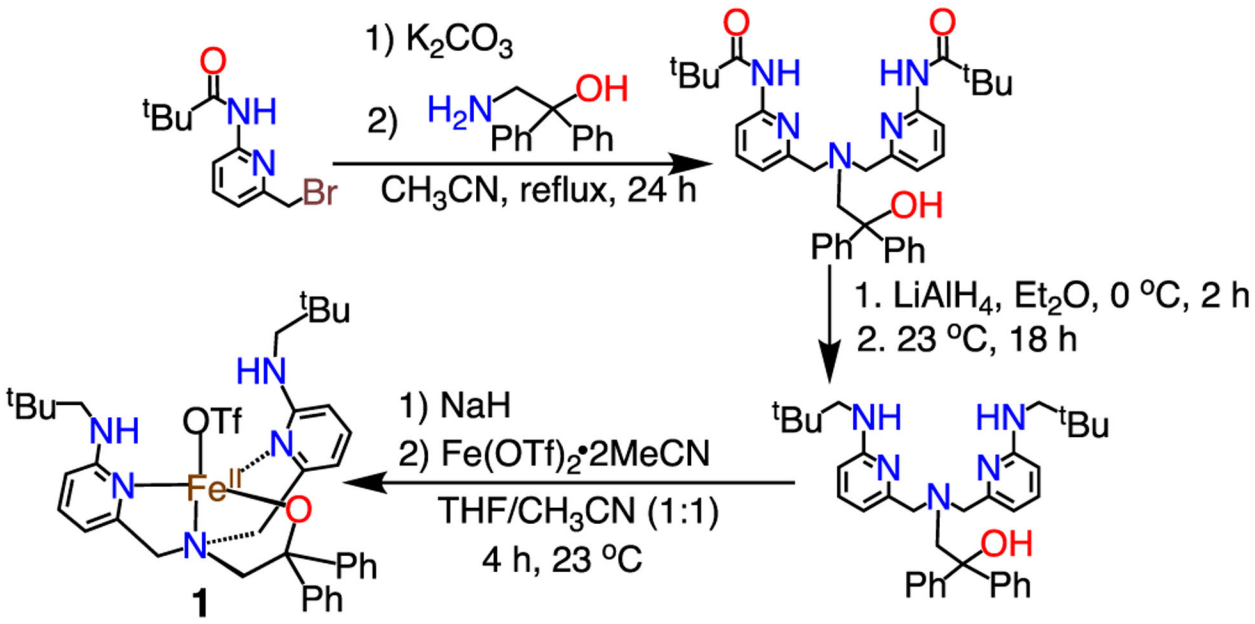

Scheme 2.
Synthesis of BNPA^{Ph2}OH and Complex 1

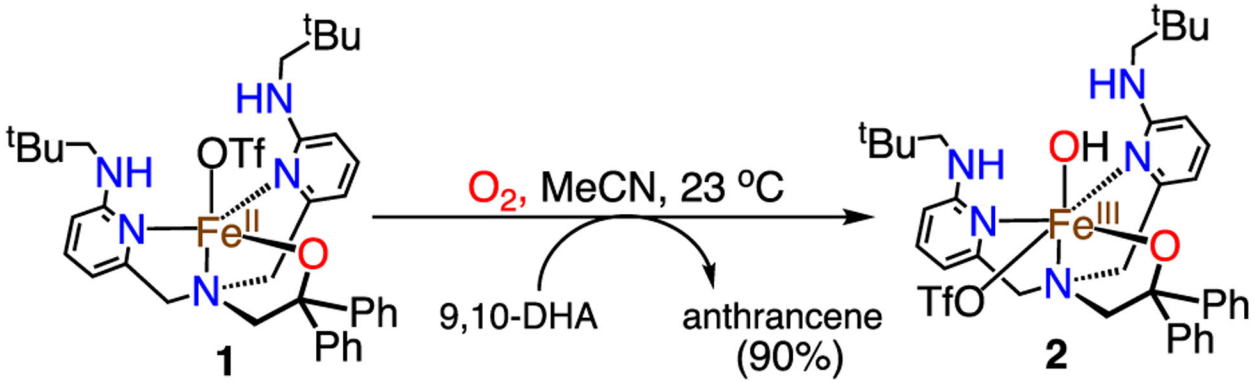

Scheme 3.
Activation of Dioxygen by 1

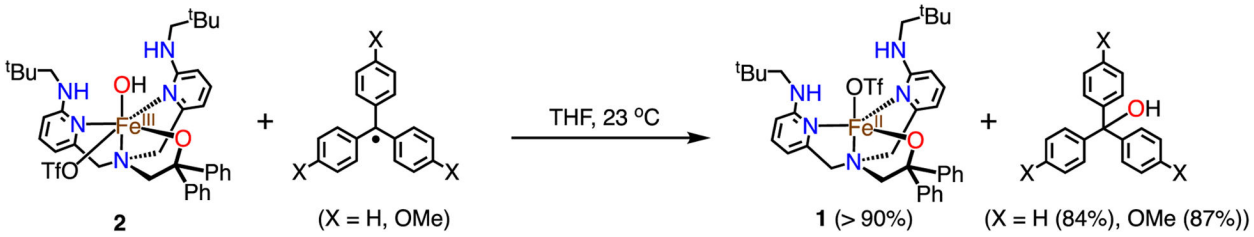

Scheme 4.
Reaction between 2 and Triarylmethyl Radicals